

---

---

# The Temperature of Nonspherical Circumstellar Dust Grains<sup>1</sup>

© 2000 N. V. Voshchinnikov\* and D. A. Semenov

*Sobolev Astronomical Institute, St. Petersburg State University,  
Bibliotechnaya pl. 2, St. Petersburg-Peterhof, 198504 Russia*

Received January 28, 2000

**Abstract**—The temperatures of prolate and oblate spheroidal dust grains in the envelopes of stars of various spectral types are calculated. Homogeneous particles with aspect ratios  $a/b \leq 10$  composed of amorphous carbon, iron, dirty ice, various silicates, and other materials are considered. The temperatures of spherical and spheroidal particles were found to vary similarly with particle size, distance to the star, and stellar temperature. The temperature ratio  $T_d(\text{spheroid})/T_d(\text{sphere})$  depends most strongly on the grain chemical composition and shape. Spheroidal grains are generally colder than spherical particles of the same volume; only iron spheroids can be slightly hotter than iron spheres. At  $a/b \approx 2$ , the temperature differences do not exceed 10 %. If  $a/b \gtrsim 4$ , the temperatures can differ by 30–40 %. For a fixed dust mass in the medium, the fluxes at wavelengths  $\lambda \gtrsim 100 \mu\text{m}$  are higher if the grains are nonspherical, which gives over estimated dust masses from millimeter observations. The effect of grain shape should also be taken into account when modeling Galactic-dust emission properties, which are calculated when searching for fluctuations of the cosmic microwave background radiation in its Wien wing.

*Keywords:* interstellar medium, circumstellar shells

## 1. INTRODUCTION

The observed infrared and submillimeter emission from interstellar clouds, circumstellar envelopes, and galaxies is generally thermal emission of dust heated by stellar radiation or shock waves. When infrared spectra of these objects are computed, the dust temperature must be calculated. This temperature is also used to determine the mass and thermal balance of the matter in various objects and is important for the formation of molecules on the grain surfaces.

Calculations of the interstellar dust temperature were initiated in the 1940s [see van de Hulst (1949) for a discussion]. The equilibrium temperature of spherical dust grains is commonly considered (see, e.g., Mathis *et al.* 1983). However, it has been known for fifty years [since the discovery of interstellar polarization by Hiltner (1949), Hall (1949), and Dombrovskii (1949)] that there are nonspherical aligned particles in the interstellar medium.

<sup>1</sup> To the memory of Gennadii Borisovich Sholomitskii, an enthusiast for research in the field of infrared and submillimeter astronomy.

\*E-mail address for contacts: nvv@dust.astro.spbu.ru.

Nonspherical particles appear to be also present in the circumstellar dust shells. The variations in the position angle of linear polarization with time and wavelength observed in red giants provide circumstantial evidence for this (Dyck and Jennings 1971; Shawl 1975). Even after correction for the interstellar polarization, the position-angle difference in the blue and in the red can reach  $20^\circ - 60^\circ$ . This behavior is very difficult to explain in terms of the model of a single star with a shell containing spherical particles alone. If, alternatively, there are nonspherical grains in the shell, then variations in the degree and direction of grain alignment may result in the observable variations of the polarization angle.

The first attempt to take into account the effect of the shape of interstellar grains on their temperature was made by Greenberg and Shah (1971). These authors considered metallic and dielectric Rayleigh spheroids and infinite ice cylinders of  $0.1\text{-}\mu\text{m}$  radius. They concluded that nonspherical particles were approximately 10% colder than spheres, a result that entered the books on interstellar dust (Whittet 1992).

Recently, Fogel and Leung (1998) have computed the infrared radiation of fractal dust grains produced by two processes of stochastic growth and composed of amorphous carbon and silicate. They concluded that the temperature of nonspherical particles was typically 10–20% lower than that of spherical ones, which results in a longward shift of the maximum of the object's radiation. Fogel and Leung (1998) proposed to consider the fractal particle size as a parameter of the grain shape, but they ignored the effects of alignment.

Here, we study in detail the dependence of the temperature of spheroidal circumstellar dust grains on their shape and alignment. We consider prolate and oblate particles of various sizes, which are composed of a variety of absorbing and dielectric materials and which lie at various distances from stars with various temperatures. The nonsphericity effect of interstellar dust grains on their temperature was discussed by Voshchinnikov *et al.* (1999).

## 2. THE MODEL

### 2.1. The Radiation Field

Dust particles are present in the envelopes of late-type stars (red giants and supergiants) and hotter stars, such as Herbig Ae/Be stars. Dust grains are heated mainly by the absorption of stellar radiation. As was pointed out by Lamy and Perrin (1997), in some cases, it is important to take into account the star's true spectral energy distribution as well. In addition, in the outer regions of optically thick dust shells, the maximum in the energy distribution is redshifted (see, e.g., Bagnulo *et al.* 1995). For simplicity, however, we assume the energy distribution to be a blackbody one with an effective temperature  $T_\star$ . Since we are going to compare the temperatures of particles under the same conditions, this assumption is of no fundamental importance.

In most cases, we take the stellar temperature to be  $T_\star = 2500$  K, typical of late-type giants and supergiants (Pégourié 1987; Lorenz-Martins and Lefévre 1995). The effects of variations in  $T_\star$  are discussed in subsection 4.5.

### 2.2. Dust Particles

**Chemical composition.** Particles of amorphous carbon and amorphous silicates are most commonly considered as the major sources of the infrared radiation observed from carbon and oxygen stars, respectively. Evidence in support of these materials follows both from theoretical models of dust formation (Gail and Sedlmayr 1984) and from laboratory experiments (Jäger *et al.* 1994).

The specific type of silicate or carbon material in the circumstellar medium is very difficult to determine. In addition, there is most likely a mixture of various dust components in the shells simultaneously. For example, bands of silicon carbide, sulfide silicates, and even amorphous silicates were detected in the spectra of some carbon stars (Baron *et al.* 1987; Goebel and Moseley; Little-Marenin 1986). Several emission bands found in the spectra of carbon stars were identified with crystalline silicates (Waters *et al.* 1999). Finally, iron and oxide particles can apparently condense in circumstellar envelopes irrespective of the C/O ratio.

In our modeling, we used the six materials that were previously chosen by Il'in and Voshchinnikov (1998) when considering the effect of radiation pressure on dust grains in the envelopes of late-type stars: amorphous carbon, iron, and magnetite ( $\text{Fe}_3\text{O}_4$ ) as examples of strongly absorbing materials, as well as astronomical silicate (astrosil), transparent glassy pyroxene, and artificial dirty silicate (Ossenkopf *et al.* 1992; OHM silicate) as silicates of various types. References to the papers from which we took the optical constants of these materials can be found in Il'in and Voshchinnikov (1998).<sup>2</sup> This set of materials was extended to include carbon material (cellulose), which was produced by pyrolysis at the temperature of  $1000^\circ\text{C}$  (cel1000; Jäger *et al.* 1998), and dirty ice, which was used in the classical study by Greenberg and Shah (1971). In the latter case, the imaginary part of the refractive index was chosen to be  $k = 0.02$  in the wavelength range  $0.17\text{--}1.2\text{ }\mu\text{m}$ , as was done by Greenberg (1970, 1971).

**Shape.** The formation of only spherical particles in the envelopes of late-type stars has been considered thus far (see, e.g., Draine 1981; Gail and Sedlmayr 1985; Fadeyev 1987; Fleischer *et al.* 1992; Cadwell *et al.* 1994). The theory of nucleation and growth of nonspherical particles is still at the initial stage of its development.

We assume the circumstellar dust grains to be prolate and oblate homogeneous spheroids with aspect ratios  $a/b$  ( $a$  and  $b$  are the spheroid semimajor and semiminor axes, respectively). By varying  $a/b$ , we can model the particle shape over a wide range: from spheres to needles and disks.

**Size.** Dust grains form and grow in the envelopes of late-type stars. They range in size from tiny particles to particles with radii up to  $1\text{ }\mu\text{m}$  or more [see Lafon and Berruyer (1991) for a discussion]. The upper limit of the grain size distribution is uncertain and is the subject of debate. However, it follows from model calculations that, in general, the particle size in oxygen stars is larger than that in carbon ones (Jura 1994, 1996; Bagnulo *et al.* 1995).

In order to compare the optical properties of particles of the same volume but different shape, it is convenient to characterize the particle size by the radius  $r_V$  of a sphere equal in volume to a spheroid. The spheroid semimajor axis is related to  $r_V$  by

$$a = r_V \left( \frac{a}{b} \right)^{2/3} \quad (1)$$

for prolate spheroids and by

$$a = r_V \left( \frac{a}{b} \right)^{1/3} \quad (2)$$

for oblate spheroids. In our calculations, we considered particles with  $r_V = 0.005\text{--}0.5\text{ }\mu\text{m}$ .

**Structure.** The dust grains growing in circumstellar shells can be fluffy or porous. To model the effect of porosity, we used Bruggeman's rule (Bohren and Huffman 1986) and obtained the

---

<sup>2</sup>Data on the refractive indices can also be extracted from an electronic database of optical constants (Henning *et al.* 1999) via Internet at <http://www.astro.spbu.ru/JPDOC/entry.html>.)

mean effective dielectric function  $\varepsilon_{\text{eff}}$  of an aggregate composed of  $n$  materials with dielectric functions  $\varepsilon_i$ ,

$$\sum_{i=1}^n f_i \frac{\varepsilon_i - \varepsilon_{\text{eff}}}{\varepsilon_i + 2\varepsilon_{\text{eff}}} = 0, \quad (3)$$

where  $f_i$  is the volume fraction occupied by the material of type  $i$ . The temperature is calculated for compact particles with  $\varepsilon_{\text{eff}}$ . We considered spheroids composed of vacuum ( $\varepsilon = 1$ ) and cellulose with vacuum fractions from 0 to 0.9.

**Orientation.** Collisions of dust grains with atoms and molecules cause rapid grain rotation with angular velocities  $> 10^5 \text{ s}^{-1}$ . Interstellar particles are believed to rotate around the direction of maximum moment of inertia, and, in general, the angular momentum is parallel to the magnetic field (Spitzer 1981). Circumstellar particles can be aligned by anisotropic radiation or gas fluxes (Dolginov *et al.* 1979). Radial grain motion in the shells must apparently cause particle rotation in the planes containing the radius vector. However, nonradial gas flows or the helical circumstellar magnetic fields produced by stellar rotation (see, e.g., Woitke *et al.* 1993) can also result in a different grain alignment.

In our modeling, we considered two types of grain orientation: particles randomly oriented in space (3D orientation) and in a plane (2D orientation or complete rotational orientation). In the latter case, the major axis of a rotating spheroid always lies in the same plane. The angle  $\Omega$  between the particle angular velocity and the wave vector of the incident radiation is a model parameter ( $0^\circ \leq \Omega \leq 90^\circ$ ).

### 3. BASIC EQUATIONS

Let us consider a dust grain at distance  $R$  from a star of radius  $R_*$  and temperature  $T_*$ . The stellar radiation is assumed to be unpolarized. The equilibrium grain temperature  $T_d$  can be determined from Kirchoff's law by solving the energy balance equation for the absorbed and emitted energy ( $\text{erg s}^{-1}$ )

$$W \int_0^\infty \overline{C}_{\text{abs}}(\lambda) \pi B_\lambda(T_*) d\lambda = \int_0^\infty \overline{C}_{\text{em}}(\lambda) \pi B_\lambda(T_d) d\lambda, \quad (4)$$

where  $\overline{C}_{\text{abs}}(\lambda)$  and  $\overline{C}_{\text{em}}(\lambda)$  are the orientation-averaged absorption and emission cross sections,  $\pi B_\lambda(T)$  is the blackbody flux with temperature  $T$  ( $\text{erg cm}^{-2} \text{s}^{-1} \mu\text{m}^{-1}$ ), and  $W = R_*^2/R^2$  is the radiation dilution factor.

For particles randomly oriented in space, the absorption cross sections must be averaged over all orientations:

$$\overline{C}_{\text{abs}}^{\text{3D}} = \int_0^{\pi/2} \frac{1}{2} \left[ Q_{\text{abs}}^{\text{TM}}(m_\lambda, r_V, \lambda, a/b, \alpha) + Q_{\text{abs}}^{\text{TE}}(m_\lambda, r_V, \lambda, a/b, \alpha) \right] G(\alpha) \sin \alpha d\alpha. \quad (5)$$

Here,  $m_\lambda$  is the refractive index of the grain material ( $m_\lambda = \varepsilon_\lambda^{1/2}$ ),  $\alpha$  is the angle between the spheroid rotation axis and the wave vector ( $0^\circ \leq \alpha \leq 90^\circ$ ), and  $G$  is the geometric cross section of the spheroid (the area of the particle shadow):

$$G(\alpha) = \pi r_V^2 \left( \frac{a}{b} \right)^{-2/3} \left[ \left( \frac{a}{b} \right)^2 \sin^2 \alpha + \cos^2 \alpha \right]^{1/2} \quad (6)$$

for prolate spheroids and

$$G(\alpha) = \pi r_V^2 \left( \frac{a}{b} \right)^{2/3} \left[ \left( \frac{a}{b} \right)^{-2} \sin^2 \alpha + \cos^2 \alpha \right]^{1/2}. \quad (7)$$

for oblate spheroids.

In the case of complete rotational orientation, the absorption cross sections are averaged over all rotation angles  $\phi$ . For prolate spheroids, this yields

$$\bar{C}_{\text{abs}}^{\text{2D}}(\Omega) = \frac{2}{\pi} \int_0^{\pi/2} \frac{1}{2} [Q_{\text{abs}}^{\text{TM}}(m_\lambda, r_V, \lambda, a/b, \alpha) + Q_{\text{abs}}^{\text{TE}}(m_\lambda, r_V, \lambda, a/b, \alpha)] G(\alpha) d\phi, \quad (8)$$

where the angle  $\alpha$  is related to  $\Omega$  and  $\phi$  ( $\cos \alpha = \sin \Omega \cos \phi$ ). For oblate spheroids arbitrarily oriented in a plane, we have  $\Omega = \alpha$  and

$$\bar{C}_{\text{abs}}^{\text{2D}}(\Omega) = \frac{1}{2} [Q_{\text{abs}}^{\text{TM}}(m_\lambda, r_V, \lambda, a/b, \Omega) + Q_{\text{abs}}^{\text{TE}}(m_\lambda, r_V, \lambda, a/b, \Omega)] G(\Omega). \quad (9)$$

The energy emitted by a particle is proportional to its surface area. The emission cross section can then be calculated as follows:

$$\bar{C}_{\text{em}} = S \int_0^{\pi/2} \frac{1}{2} [Q_{\text{abs}}^{\text{TM}}(m_\lambda, r_V, \lambda, a/b, \alpha) + Q_{\text{abs}}^{\text{TE}}(m_\lambda, r_V, \lambda, a/b, \alpha)] \sin \alpha d\alpha, \quad (10)$$

where

$$S = 2\pi r_V^2 \left[ \left(\frac{a}{b}\right)^{-2/3} + \left(\frac{a}{b}\right)^{1/3} \frac{\arcsin(e)}{e} \right] \quad (11)$$

for prolate spheroids and

$$S = 2\pi r_V^2 \left[ \left(\frac{a}{b}\right)^{2/3} + \left(\frac{a}{b}\right)^{-4/3} \frac{\ln[(1+e)/(1-e)]}{2e} \right] \quad (12)$$

for oblate spheroids,  $e = \sqrt{1 - (a/b)^{-2}}$ .

In Eqs. (5), (8), (9), and (10), the superscripts TM and TE refer to two polarizations of the incident radiation (TM and TE modes). The efficiency factors  $Q_{\text{abs}}^{\text{TM,TE}}$  can be calculated using an exact solution to the problem of diffraction of a plane electromagnetic wave by a homogeneous spheroid by separation of variables method [see Voshchinnikov and Farafonov (1993) for more detail]. We used the benchmark results of calculations of the efficiency factors from Voshchinnikov *et al.* (2000) to thoroughly test the computational program.

#### 4. RESULTS AND DISCUSSION

In this section, we discuss the dependence of the spheroidal-grain temperature on model parameters: the particle chemical composition, size, shape, and orientation, as well as the stellar temperature and distance to the star. We also consider the effects of porosity and partial polarization of the incident radiation on the particle temperature. Since the main goal of our study is to analyze the effects of change in the particle shape, we compare the temperature ratio of spheroidal and spherical particles of the same volume.

##### 4.1. A Graphical Method of Temperature Determination and a Blackbody Model

This method, proposed by Greenberg (1970, 1971), allows the causes of temperature differences between dust grains with different characteristics to be clearly established if the particles are assumed to be in an isotropic radiation field. Their temperature can then be determined by solving the following equation of thermal balance:

$$W \int_0^\infty \bar{C}_{\text{abs}}(\lambda) 4\pi B_\lambda(T_\star) d\lambda = \int_0^\infty \bar{C}_{\text{em}}(\lambda) \pi B_\lambda(T_d) d\lambda. \quad (13)$$

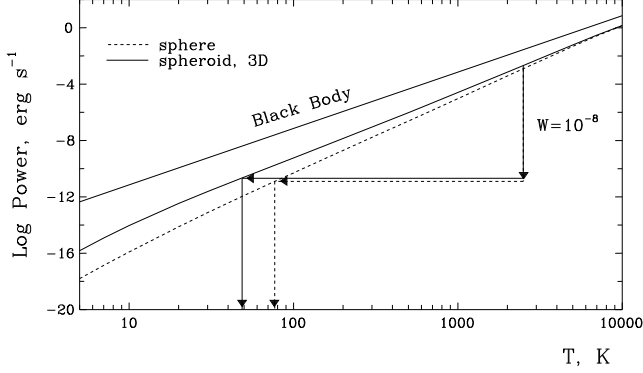


Figure 1: The power absorbed (emitted) by dust particles with  $r_V = 0.01 \mu\text{m}$  in an isotropic radiation field. The straight line corresponds to a blackbody. The curves refer to spherical and prolate spheroidal ( $a/b = 10$ , 3D orientation) cellulose (cel1000) particles. A graphical method of determining the grain temperature is shown for  $T_* = 2500 \text{ K}$  and  $W = 10^{-8}$ . In this case, the temperatures of spherical and spheroidal particles and a blackbody are respectively,  $T_d(\text{sphere}) = 76.8 \text{ K}$ ,  $T_d^{3D} = 48.7 \text{ K}$ , and  $T_d^{\text{BB}} = 2500(10^{-8})^{1/4} = 25 \text{ K}$ .

If the spheroidal particles are randomly oriented in space (3D orientation), then numerical estimates show that

$$\overline{C}_{\text{abs}}^{3D} \approx \frac{\overline{C}_{\text{em}}}{4} \quad (14)$$

The integrals on the left- and right-hand sides of Eq. (13) then depend on the temperature  $T$  alone (for given particle chemical composition, size, and shape).

Figure 1 shows the power for the absorbed (emitted) radiation (in  $\text{erg s}^{-1}$ ) for spheres and spheroids of the same volume ( $r_V = 0.01 \mu\text{m}$ ) composed of cellulose (cel1000). The method of temperature determination is indicated by arrows: from the point on the curve corresponding to the stellar temperature ( $T_* = 2500 \text{ K}$ ), we drop a perpendicular whose length is determined by the radiation dilution factor and then find the point of intersection of the horizontal segment with the same curve for the power. This point gives the dust grain temperature  $T_d$  determined from the equation of thermal balance (13).

It follows from Fig. 1 that the different temperatures of spheres and spheroids result from different particle emissivities at low  $T$ . The differences are most noticeable for cellulose. For other materials, the pattern of dependence is preserved: the emissivity of spheroidal particles at low temperatures is larger than that for spheres and closer to the blackbody one (see Fig. 2). Only iron particles constitute an exception: spheres composed of them at  $T \lesssim 30 \text{ K}$  emit more energy than spheroids with  $a/b \simeq 2 - 6$  but less energy than spheroids with  $a/b \gtrsim 8$  (Fig. 3).

The straight lines in the upper parts of Figs. 2 and 3 refer to a blackbody, for which the emissivity is proportional to  $T^4$ , and the absorption efficiency factors are equal to unity,

$$Q_{\text{abs}}^{\text{TM}} = Q_{\text{abs}}^{\text{TE}} = 1. \quad (15)$$

Using Eq. (15) and Stefan–Boltzmann’s law, instead of Eq. (13) we obtain for the 3D orientation

$$4W\overline{G}^{3D}\sigma T_*^4 = S\sigma T_d^4. \quad (16)$$

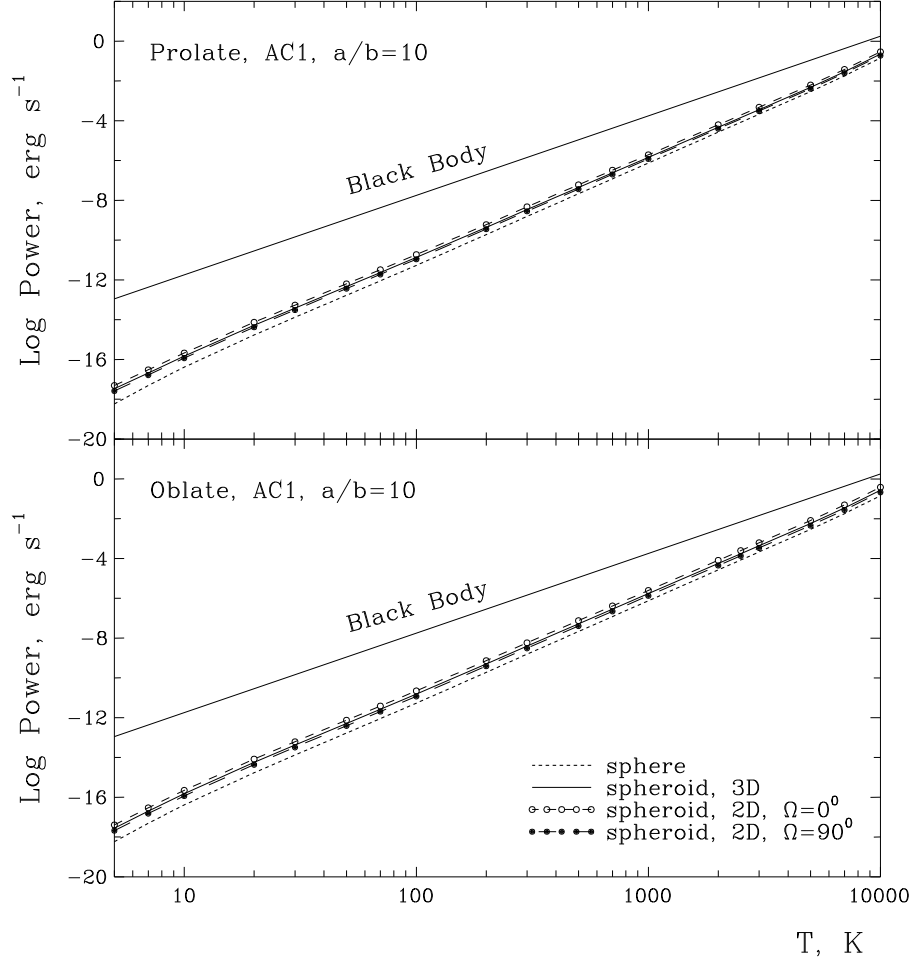


Figure 2: The power absorbed by dust particles with  $r_V = 0.01 \mu\text{m}$  in an anisotropic radiation field. The curves refer to spherical, prolate, and oblate spheroidal amorphous carbon (AC1) particles with  $a/b = 10$ . The straight line corresponds to a blackbody.

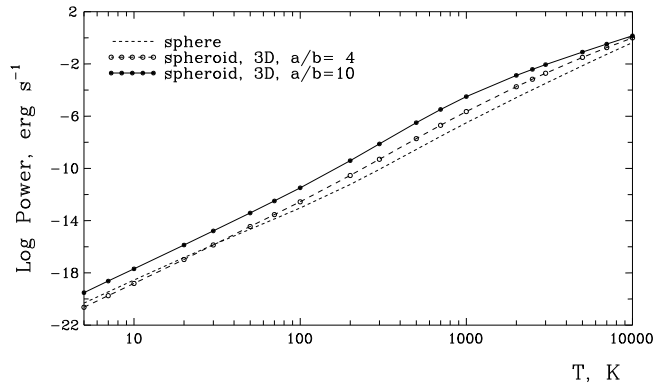


Figure 3: The power absorbed by iron dust particles with  $r_V = 0.01 \mu\text{m}$  in an anisotropic radiation field.

Considering that the mean projection area of any convex figure is a quarter of its surface area (see, e.g., Hildebrand 1983),<sup>3</sup>

$$\overline{G}^{3D} = \frac{S}{4}, \quad (17)$$

we have for spheres and spheroids randomly oriented in space

$$T_d^{BB} = T_\star W^{1/4}. \quad (18)$$

For the 2D orientation, the blackbody temperature is

$$T_d^{BB} = T_\star \left( \frac{4W\overline{G}^{2D}(\Omega)}{S} \right)^{1/4}. \quad (19)$$

Expressions for the mean cross sections in the case of complete rotational orientation were derived by Il'in and Voshchinnikov (1998):

$$\overline{G}^{2D}(\Omega) = \pi r_V^2 \frac{2}{\pi} E \left( \left[ 1 - \left( \frac{a}{b} \right)^{-2} \right] \sin^2 \Omega \right) \left( \frac{a}{b} \right)^{1/3} \quad (20)$$

for prolate spheroids and

$$\overline{G}^{2D}(\Omega) = G(\Omega) \quad (21)$$

for oblate spheroids. In Eq. (20), the complete elliptic integral of the second kind is denoted by  $E(m)$ . Based on Eqs. (20) and (21), we can easily determine the blackbody-temperature ratios for the two extreme cases of 2D orientation ( $\Omega = 0^\circ$   $\Omega = 90^\circ$ ):

$$\frac{T_d^{BB}(\Omega = 0^\circ)}{T_d^{BB}(\Omega = 90^\circ)} = \left( \frac{\overline{G}^{2D}(\Omega = 0^\circ)}{\overline{G}^{2D}(\Omega = 90^\circ)} \right)^{1/4} = \left( \frac{\pi}{2E \left( 1 - \left( \frac{a}{b} \right)^{-2} \right)} \right)^{1/4} \quad (22)$$

for prolate spheroids and

$$\frac{T_d^{BB}(\Omega = 0^\circ)}{T_d^{BB}(\Omega = 90^\circ)} = \left( \frac{a}{b} \right)^{1/4} \quad (23)$$

for oblate spheroids. We can also calculate the temperature ratio of a spheroid for the 2D orientation and a sphere (or a spheroid for the 3D orientation):

$$\frac{T_d^{BB}(\Omega)}{T_d^{BB}(\text{sphere, 3D})} = \left( \frac{4\overline{G}^{2D}(\Omega)}{S} \right)^{1/4}. \quad (24)$$

Note that Eqs. (22)–(24) allow the geometric effects on the temperature of nonspherical dust grains to be estimated. For example,  $T_d^{BB}(\Omega = 0^\circ)/T_d^{BB}(\text{sphere}) = 1.06$  (1.18) for  $a/b = 10$  and  $T_d^{BB}(\Omega = 90^\circ)/T_d^{BB}(\text{sphere}) = 0.95$  (0.66) for prolate (oblate) spheroids.

#### 4.2. Dependence on the Distance from the Star

The temperature of particles of any shape decreases with distance from the heating source (star). However, the temperature ratio of nonspherical and spherical particles varies over a narrow

---

<sup>3</sup>Eq. (17) for prolate and oblate spheroids can be proved by directly integrating Eqs. (6) and (7).

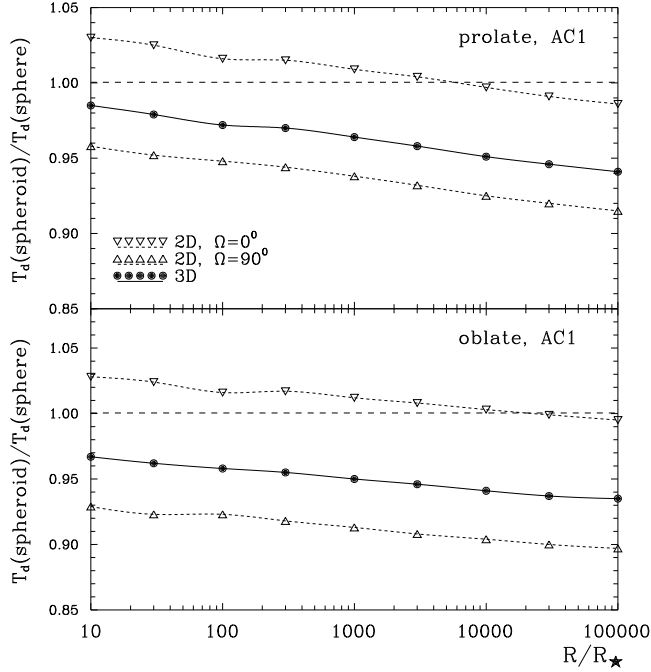


Figure 4: The temperature ratio of prolate and oblate spheroidal ( $a/b = 4$ ) and spherical amorphous carbon (AC1) grains with  $r_V = 0.01 \mu\text{m}$  at various distances from a star with  $T_\star = 2500 \text{ K}$ . The sphere temperature is  $T_d(\text{sphere}) = 780.6 \text{ K}, 318.0 \text{ K}, 130.8 \text{ K}, 52.3 \text{ K}$  and  $20.8 \text{ K}$  for  $R = 10, 10^2, 10^3, 10^4$  and  $10^5 R_\star$ , respectively.

range. As follows from Fig. 4, which shows the results of our calculations for amorphous carbon particles, this ratio decreases approximately by 5% as the distance to the star increases from  $10$  to  $10^5 R_\star$ . In this case, the sphere temperature decreases from  $780.6$  to  $20.8 \text{ K}$ . Given the insignificant variation of  $T_d(\text{spheroid})/T_d(\text{sphere})$  with  $R$ , below we consider the results only for  $R = 10^4 R_\star$  ( $W = 10^{-8}$ ).

#### 4.3. Dependence on the Grain Size

The temperature variations of carbon and silicate dust grains with particle radius are given in Tables 1 and 2. As  $r_V$  increases, the particle temperature slightly rises and then begins to fall, as was also noted previously (Greenberg 1970). The temperature of spheroidal particles is always slightly lower than that of spherical ones; the difference can reach 10% at  $a/b = 4$ . The temperature difference between spheres and spheroids is largest for the 2D orientation and  $\Omega = 90^\circ$ . Note also that, since  $T_d$  for spheres and spheroids vary with  $r_V$  similarly, the temperature ratio is almost independent of  $r_V$ .

#### 4.4. Dependence on the Grain Shape and Chemical Composition

The effects of the chemical composition and shape of dust grains on their temperature are most significant compared to the variations of other model parameters. These effects are illustrated in Figs. 5 and 6, which show the temperature ratios of spheroids and spheres for particles with metallic and dielectric properties, respectively. The variations of  $T_d(\text{spheroid})/T_d(\text{sphere})$  have the following general tendency: this ratio decreases with increasing  $a/b$  and absorptive material properties, with the effect increasing. Besides, the following inequality holds for particles of the

Table 1: The temperatures (in K) of spherical and spheroidal ( $a/b = 4$ ) amorphous carbon grains;  $T_\star = 2500$  K,  $R = 10\,000 R_\star$

$r_V, \mu\text{m}$	Sphere	P			rotate spheroid			O			blate spheroid		
		2D, $\Omega = 0^\circ$	2D, $\Omega = 90^\circ$	3D	2D, $\Omega = 0^\circ$	2D, $\Omega = 90^\circ$	3D	2D, $\Omega = 0^\circ$	2D, $\Omega = 90^\circ$	3D	2D, $\Omega = 0^\circ$	2D, $\Omega = 90^\circ$	3D
0.005	52.3	52.1	48.4	49.7	52.4	52.4	47.2	47.2	47.3	49.2	47.3	47.3	49.2
0.010	52.3	52.2	48.4	49.8	52.4	52.4	47.2	47.2	47.3	49.2	47.3	47.3	49.2
0.020	52.4	52.3	48.5	49.9	52.6	52.6	47.4	47.4	47.4	49.3	47.4	47.4	49.3
0.030	52.6	52.5	48.7	50.1	52.8	52.8	47.6	47.6	47.6	49.5	47.6	47.6	49.5
0.050	53.3	53.2	49.2	50.6	53.3	53.3	48.2	48.2	48.2	50.1	48.2	48.2	50.1
0.100	56.0	54.9	51.0	52.4	54.8	54.8	50.4	50.4	50.4	52.0	50.4	50.4	52.0
0.200	61.1	55.5	54.4	54.7	54.6	54.6	54.3	54.3	54.3	54.3	54.3	54.3	54.3
0.300	62.3	55.0	55.7	55.4	53.6	53.6	55.4	55.4	55.4	54.6	55.4	55.4	54.6
0.500	60.2	53.5	54.3	54.0	51.8	51.8	53.6	53.6	53.6	52.9	53.6	53.6	52.9

Table 2: The temperatures (in K) of spherical and spheroidal ( $a/b = 4$ ) astronomical silicate grains  $T_\star = 2500$  K,  $R = 10\,000 R_\star$

$r_V, \mu\text{m}$	Sphere	P			rotate spheroid			O			blate spheroid		
		2D, $\Omega = 0^\circ$	2D, $\Omega = 90^\circ$	3D	2D, $\Omega = 0^\circ$	2D, $\Omega = 90^\circ$	3D	2D, $\Omega = 0^\circ$	2D, $\Omega = 90^\circ$	3D	2D, $\Omega = 0^\circ$	2D, $\Omega = 90^\circ$	3D
0.005	34.9	31.9	30.6	31.2	32.6	32.6	30.5	30.5	30.5	31.3	30.5	30.5	31.3
0.010	34.9	31.9	30.6	31.1	32.7	32.7	30.5	30.5	30.5	31.3	30.5	30.5	31.3
0.020	34.9	31.9	30.7	31.1	32.7	32.7	30.6	30.6	30.6	31.4	30.6	30.6	31.4
0.030	35.0	32.0	30.7	31.2	32.8	32.8	30.6	30.6	30.6	31.4	30.6	30.6	31.4
0.050	35.2	32.2	30.9	31.4	32.9	32.9	30.8	30.8	30.8	31.6	30.8	30.8	31.6
0.100	36.0	32.8	31.5	32.0	33.5	33.5	31.5	31.5	31.5	32.2	31.5	31.5	32.2
0.200	38.2	33.5	33.0	33.1	33.8	33.8	33.3	33.3	33.3	33.4	33.3	33.3	33.4
0.300	39.6	33.7	34.4	34.0	33.6	33.6	34.7	34.7	34.7	34.2	34.7	34.7	34.2
0.500	40.5	34.1	35.4	34.9	33.4	33.4	35.9	35.9	35.9	34.8	35.9	35.9	34.8

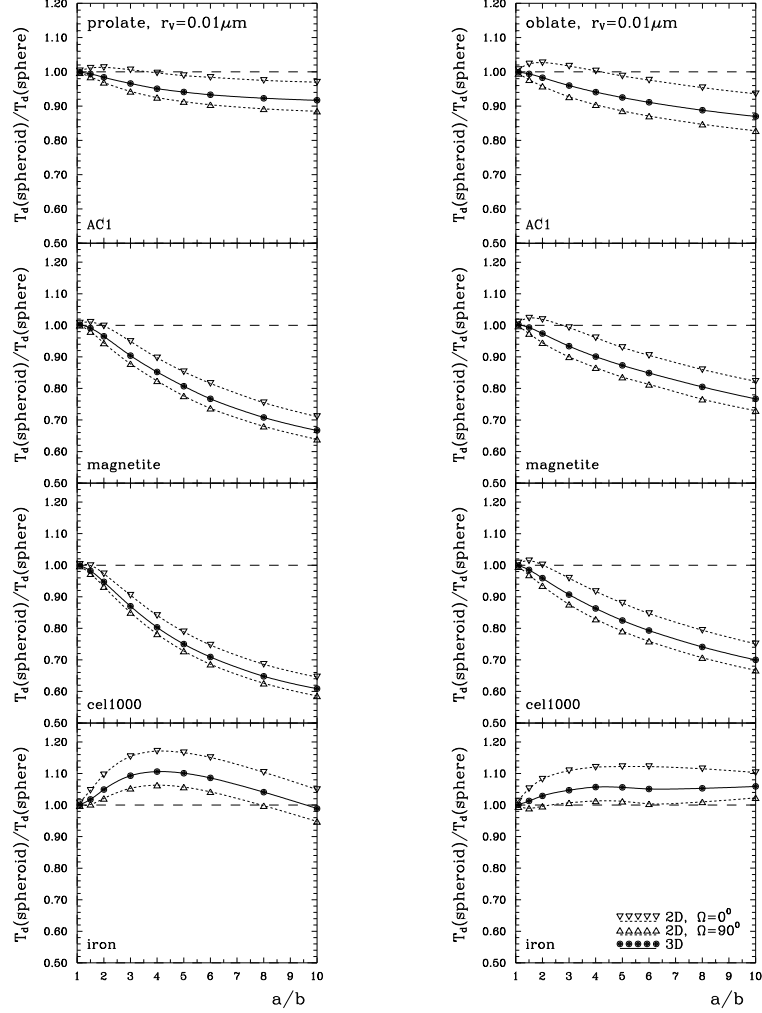


Figure 5: The temperature ratio of prolate and oblate spheroidal and spherical grains composed of various materials with metallic properties;  $T_\star = 2500$  K,  $r_V = 0.01 \mu\text{m}$ , and  $R = 10^4 R_\star$ . The sphere temperature is  $T_d(\text{sphere}) = 52.3$  K, 63.0 K, 59.2 K, and 120.0 K for particles of amorphous carbon, magnetite, cellulose, and iron, respectively.

same volume:

$$T_d(\text{sphere}) > T_d^{2\text{D}}(\Omega = 0^\circ) > T_d^{3\text{D}} > T_d^{2\text{D}}(\Omega = 90^\circ). \quad (25)$$

The difference between prolate and oblate particles, which is noticeable in Figs. 5 and 6, is determined by different optical properties of the particles [see Voshchinnikov and Farafonov (1993) for more detail]. If we restrict ourselves to  $a/b \lesssim 4$ , then it is easy to see that the dielectric and metallic spheroids are, respectively, 10 % and 20 % colder than the corresponding spheres. The temperatures of prolate and oblate particles can differ by 30–40 % from the temperature of spheres (Fig. 5). If we further increase the aspect ratio  $a/b$ , then the temperature gradually ceases to drop. For example, for prolate cel1000 particles,  $T_d^{3\text{D}}/T_d(\text{sphere}) = 0.61, 0.53, 0.50$ , and 0.50 for  $a/b = 10, 20, 50$ , and 100, respectively.

The temperature behavior for iron particles is peculiar: for  $a/b \lesssim 8$ , the spheroids are 10–20 %

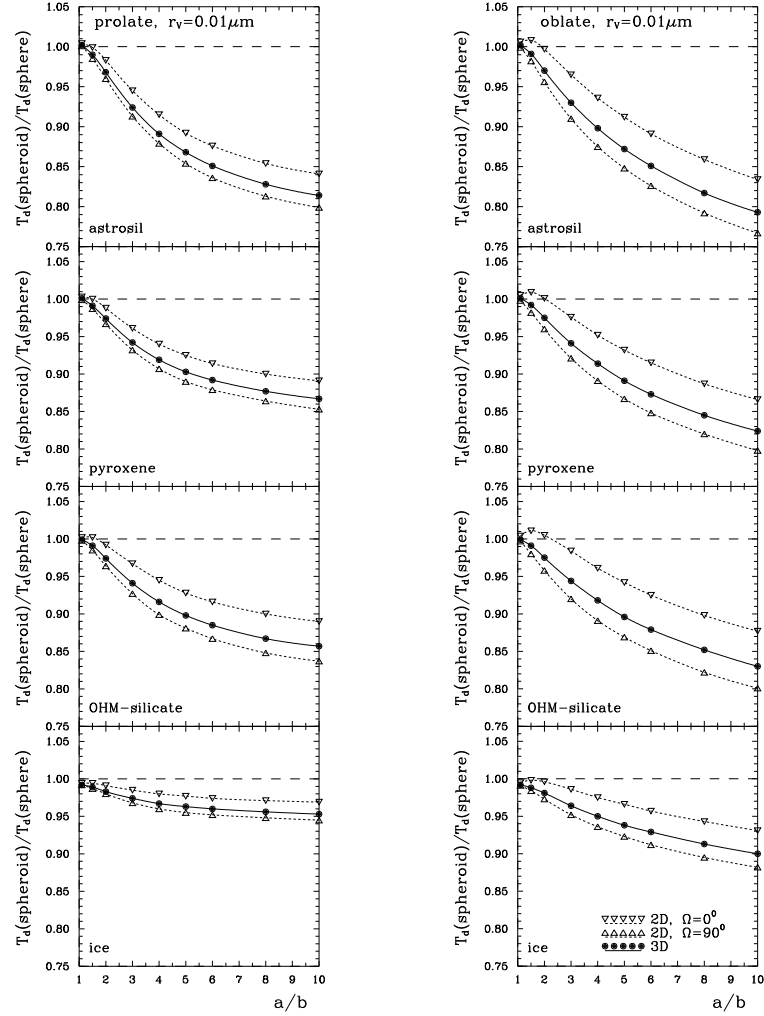


Figure 6: The same as Fig. 5 for particles with dielectric properties. The sphere temperature is  $T_d(\text{sphere}) = 34.9 \text{ K}$ ,  $24.0 \text{ K}$ ,  $42.4 \text{ K}$ , and  $33.7 \text{ K}$  for particles of astrosil, pyroxene, OHM silicate, and dirty ice, respectively.

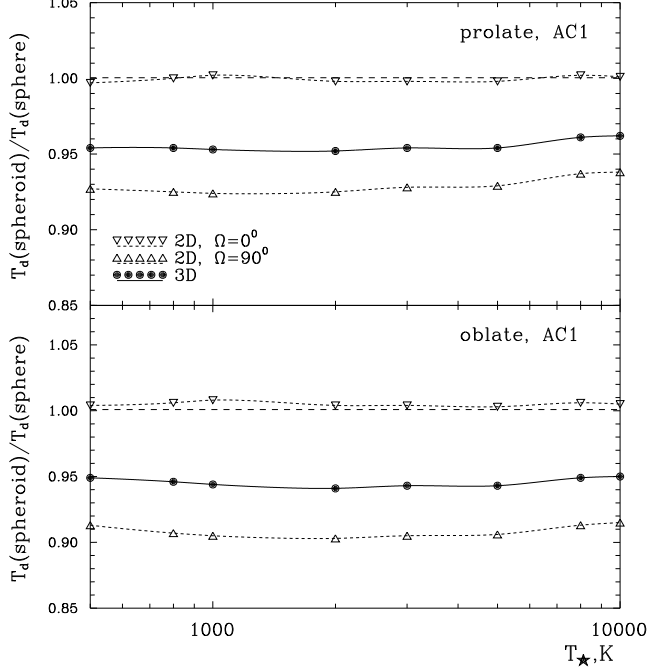


Figure 7: The temperature ratio of prolate and oblate spheroidal ( $a/b = 4$ ) and spherical amorphous carbon (AC1) grains with  $r_V = 0.01 \mu\text{m}$  at  $R = 10^4 R_\star$  from the star. The sphere temperature is  $T_d(\text{sphere}) = 10.5 \text{ K}, 20.4 \text{ K}, 63.1 \text{ K}, 106.4 \text{ K}, \text{ and } 226.4 \text{ K}$  for  $T_\star = 500 \text{ K}, 1000 \text{ K}, 3000 \text{ K}, 5000 \text{ K}, \text{ and } 10000 \text{ K}$ , respectively.

hotter than the spheres. The reason for this is seen from the behavior of the particle emissivity shown in Fig. 3.

#### 4.5. Dependence of the Stellar Temperature

Nonspherical particles may be present in the shells of stars of various spectral types and in the interplanetary medium. The effects of variations in the stellar temperature are shown in Fig. 7 for amorphous carbon particles with  $r_V = 0.01 \mu\text{m}$ . Low effective temperatures (up to 500 K) correspond to possible conditions in the outer parts of optically thick circumstellar shells. It follows from Fig. 7 that there is no effect for  $T_d(\text{spheroid})/T_d(\text{sphere})$ , although the absolute temperature varies over a fairly wide range: from  $T_d(\text{sphere}) = 10.6 \text{ K}$  at  $T_\star = 500 \text{ K}$  to  $T_d(\text{sphere}) = 226.4 \text{ K}$  at  $T_\star = 10000 \text{ K}$ .

#### 4.6. Porous Dust Grains and Polarized Incident Radiation

An increase in the fraction  $f$  of vacuum in porous particles causes a decrease in the effective refractive index, i.e., a reduction in particle absorptivity. In this case, the shape effects gradually disappear, and the temperature of spheroidal particles approaches the temperature of spheres. This effect is illustrated in Table 3, which shows that  $T_d(\text{spheroid})/T_d(\text{sphere})$  increases considerably for cellulose particles at  $f \gtrsim 0.5$ .

The aligned nonspherical particles in the inner parts of circumstellar dust shells can polarize the stellar radiation. In principle, the local linear polarization of scattered radiation can be significant. The absorption efficiency factors for the TM and TE modes must then enter into the absorption cross sections [Eqs. (5), (8), and (9)] with different weights, depending on the polarization  $P$  of the

Table 3: The temperatures (in K) of porous spherical and prolate spheroidal ( $a/b = 10$ ) cellulose (cel1000) grains;  $r_V = 0.01$ ,  $T_* = 2500$  K,  $R = 10\,000 R_*$

1 - $f$	$T_d$ (spheroid)/ $T_d$ (sphere)			$T_d$ (sphere)
	2D, $\Omega = 0^\circ$	2D, $\Omega = 90^\circ$	3D	
1.0	0.65	0.59	0.61	59.2
0.9	0.65	0.59	0.61	57.7
0.7	0.68	0.63	0.65	53.5
0.5	0.77	0.73	0.74	47.3
0.3	0.94	0.91	0.92	45.0
0.2	0.98	0.96	0.96	49.4
0.1	0.98	0.97	0.97	54.8

incident radiation. This causes an increase in the temperature of prolate spheroids if the electric vector of the incident radiation is parallel to the particle major axis (in this case,  $Q_{\text{abs}}^{\text{TM}} > Q_{\text{abs}}^{\text{TE}}$ ) and a decrease in their temperature otherwise ( $Q_{\text{abs}}^{\text{TM}} < Q_{\text{abs}}^{\text{TE}}$ ). The reverse is true for oblate spheroids. However, the effect is not too large: even at  $P = 50\%$ , the temperature of prolate spheroidal ( $a/b = 10$ ) cellulose particles varies between 33.2 and 38.3 K ( $T_d^{3D} = 36.0$  K at  $P = 0\%$ ).

The following fairly general conclusion can be drawn from what was considered above: the temperatures of spherical and nonspherical dust grains are proportional, with the proportionality coefficient being approximately the same for particles of different sizes at different distances in the envelopes of stars of diverse spectral types. This coefficient is determined only by the particle shape and by absorptive properties of the material of which they are composed.

## 5. ASTROPHYSICAL IMPLICATIONS

The dust temperature is an important parameter that determines the infrared spectra of various objects. The efficiency of grain growth and destruction, formation of molecules on the grain surfaces, and the alignment of nonspherical particles depend on  $T_d$  (Voshchinnikov 1986). Besides,  $T_d$  determines the polarized submillimeter emission of nonspherical particles (Onaka 2000) and the gas cooling rate in very dense interstellar clouds (Whitworth *et al.* 1998).

The infrared flux at wavelength  $\lambda$  emerging from an optically thin medium is proportional to the total number  $N$  of dust grains in the medium, the Planck function, which depends on the particle temperature  $T_d$ , and the emission cross section  $\overline{C}_{\text{em}}(\lambda)$ :

$$F_{\text{IR}}(\lambda) = N \frac{\overline{C}_{\text{em}}(\lambda)}{D^2} B_\lambda(T_d), \quad (26)$$

where  $D$  is the distance to the object. The quantities  $T_d$  and  $\overline{C}_{\text{em}}(\lambda)$  in Eq. (26) depend on the particle shape.

If we assume the chemical composition and sizes of all particles in the medium to be the same and if we change only the grain shape, then, when spheres are replaced by nonspherical particles, the position of the maximum in the spectrum of thermal radiation is shifted longward, because the temperature of the latter is higher (Fig. 8).

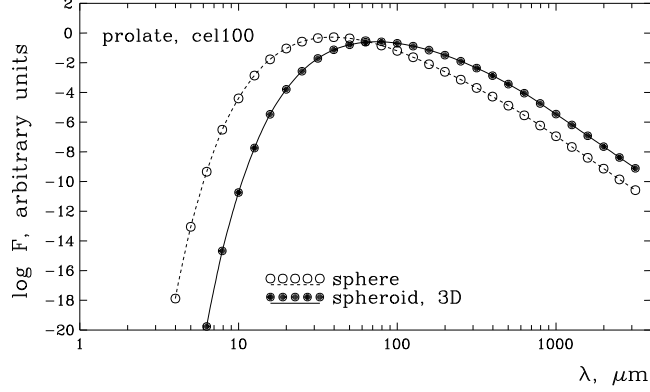


Figure 8: The normalized fluxes emerging from a medium containing the same (by mass) amount of spherical and prolate spheroidal ( $a/b = 10$ , 3D orientation) cellulose (cel1000) particles;  $r_V = 0.01 \mu\text{m}$ ,  $T_* = 2500 \text{ K}$ , and  $R = 10^4 R_*$ . The particle temperatures are  $T_d(\text{sphere}) = 59.2 \text{ K}$  and  $T_d^{3\text{D}} = 36.0 \text{ K}$ .

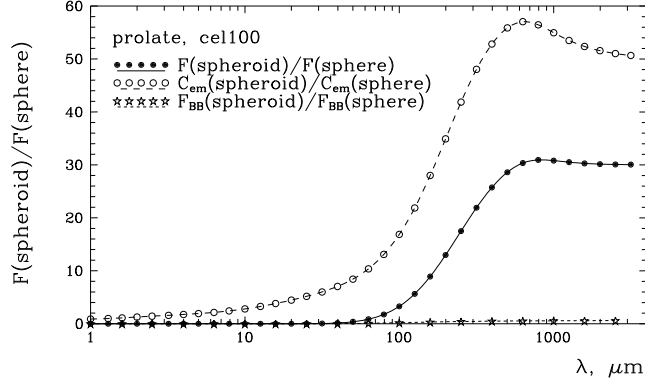


Figure 9: The same as Fig. 8 for the flux ratio. The ratios of the emission cross sections and fluxes for a blackbody are also shown. The latter are determined by the particle temperature alone.

The flux ratio is specified as follows:

$$\frac{F_{\text{IR}}^{\text{spheroid}}(\lambda)}{F_{\text{IR}}^{\text{sphere}}(\lambda)} = \frac{\bar{C}_{\text{em}}^{\text{spheroid}}(\lambda)}{\bar{C}_{\text{em}}^{\text{sphere}}(\lambda)} \frac{B_\lambda[T_d(\text{spheroid})]}{B_\lambda[T_d(\text{sphere})]}. \quad (27)$$

It is shown in Fig. 9, where the ratios of the cross sections and the Planck functions in Eq. (27) are also displayed. Despite the different particle temperatures, the Planck functions differ insignificantly. The main differences in the fluxes result from different emission cross sections  $\bar{C}_{\text{em}}(\lambda)$ : they are considerably larger for nonspherical particles at  $\lambda > \lambda_{\text{max}}$  (Fig. 9). This effect was previously noted by Ossenkopf and Henning (1994).

If the dust mass in an object is determined from the observed millimeter flux, then the Rayleigh–Jeans approximation can be used for the Planck function. For the same flux  $F_{\text{IR}}(\lambda)$ , the

dust mass depends on the particle emission cross sections and temperatures, while the ratio

$$\frac{M_d^{\text{sphere}}}{M_d^{\text{spheroid}}} = \frac{\overline{C}_{\text{em}}^{\text{spheroid}}(\lambda)}{\overline{C}_{\text{em}}^{\text{sphere}}(\lambda)} \frac{T_d(\text{spheroid})}{T_d(\text{sphere})} \quad (28)$$

shows the extent to which the values of  $M_d$  differ when changing the grain shape.

The dust mass in galaxies and molecular clouds is commonly estimated from 1.3-mm observations (Siebenmorgen *et al.* 1999). At this wavelength, the ratio of the cross sections for cellulose particles with  $a/b = 10$  (see Figs. 8 and 9) is  $\sim 50$ , and the temperature ratio is  $36.0/59.2 = 0.61$ , which gives approximately a factor of 30 larger dust mass if the particles are assumed to be spheres rather than spheroids. In other (not so extreme) cases, the dust-mass overestimate is much smaller. For example, for prolate amorphous carbon particles,  $M_d^{\text{sphere}}/M_d^{\text{spheroid}} \approx 1.2, 2.3$ , and 6.4, for  $a/b = 2, 4$ , and 10, respectively.

The degree of alignment of interstellar and circumstellar dust particles for rotational (Davies–Greenstein) orientation depends on the dust-to-gas temperature ratio: the smaller is this ratio, the more effective is the alignment of nonspherical particles (Greenberg 1970; Voshchinnikov 1986). In this case, as follows from Tables 1 and 2 and from the discussion in subsection 4.4, the nonspherical particles have a minimum temperature when the magnetic field is perpendicular to the line of sight ( $\Omega = 90^\circ$ ), i.e., when the polarization of the forward transmitted radiation is at a maximum. However, this remark more likely refers to protostellar envelopes than to interstellar particles, where the dust grains are heated by isotropic radiation.

Yet another important astrophysical process is the formation of molecules on the grain surfaces. Since the efficiency of this process strongly depends on the grain temperature, a lower temperature of nonspherical particles can significantly facilitate the formation of molecules on their surfaces [see Voshchinnikov *et al.* (1999) for a discussion].

Finally, it should be mentioned that the sublimation (along with nucleation) of spherical and nonspherical particles must take place at different distances from the star. If we consider the evaporation of ice cometary grains in the interplanetary medium, then, despite the weak shape effect for ice (see Fig. 6), the differences for spheres and spheroids prove to be noticeable enough. Ice spheres reach the sublimation temperature [ $T_d(\text{sphere}) = T_{\text{subl}} = 100$  K] and begin to evaporate at a distance  $R \approx 20$  AU from the Sun. For prolate and oblate spheroids ( $a/b = 10$ , 3D orientation), this takes place closer to the Sun: at  $R \approx 18$  and 16 AU, respectively.

## 6. CONCLUSIONS

Nonspherical interstellar and circumstellar dust grains must be slightly colder than spheres of the same volume composed of the same material. An analysis of the shape effects for spheroidal particles shows that the temperature differences do not exceed 10 % for a spheroid aspect ratio  $a/b \approx 2$ . If  $a/b \geq 4$ , then the temperature differences reach 30–40 %. Only iron spheroids can be slightly hotter than spheres. All shape effects are mainly associated with different emissivities of spherical and nonspherical particles at low temperatures. Grain porosity causes a reduction in the shape effects, whereas polarization of the incident radiation can either reduce or enhance them.

The calculated fluxes at  $\lambda \gtrsim 100 \mu\text{m}$  turn out to be higher if the grains are assumed to be nonspherical, resulting in an overestimation of the dust mass inferred from millimeter observations.

Finkbeiner and Schlegel (1999) point out that the Galactic-dust thermal emission at long wavelengths gives a major contribution to the observed background infrared radiation and must be subtracted in the search for fluctuations of the cosmic microwave background radiation in its

Wien wing. In this case, very small (in magnitude) effects compared to which the effect of grain shape is significant and must be taken into account in modeling are sought.

## ACKNOWLEDGMENTS

We wish to thank V.B. Il'in for the remarks made when reading the manuscript. This study was supported by the Volkswagen Foundation, the Program "Astronomy" and the grant of INTAS (Open Call 99/652).

## REFERENCES

1. S. Bagnulo, J.G. Doyle, I.P. Griffin, *Astron. Astrophys.* **301**, 501 (1995).
2. Y. Baron, M. de Muizon, R. Papoulier R., B. Pégourié, *Astron. Astrophys.* **186**, 271 (1987).
3. C. F. Bohren and D. R. Huffman, *Absorption and Scattering of Light by Small Particles* (Wiley, New York, 1983; Mir, Moscow, 1986).
4. B. J. Cadwell, H. Wang, E. D. Feigelson, and M. Frenklach, *Astrophys. J.* **429**, 285 (1994).
5. A. Z. Dolginov, Yu. N. Gnedin, and N. A. Silant'ev, *Propagation and Polarization of Radiation in Cosmic Medium* (Nauka, Moscow, 1979).
6. V.A. Dombrovskii, *Doklady AN Armenian SSR* **10**, 199 (1949).
7. B. T. Draine, in *Physical Processes in Red Giants*, Ed. by I. Iben and A. Renzini (Reidel, Dordrecht, 1981), p. 317.
8. H. M. Dyck and M. C. Jennings, *Astron. J.* **76**, 431 (1971).
9. Yu. A. Fadeyev, in *Circumstellar Matter: IAU Symp. No. 122*, Ed. by I. Appenzeller and C. Jordan (Reidel, Dordrecht, 1987), p. 515.
10. D. P. Finkbeiner and D. J. Schlegel, *astro-ph/9907307*.
11. A. J. Fleischer, A. Gauger, and E. Sedlmayr, *Astron. Astrophys.* **266**, 321 (1992).
12. M. E. Fogel and C. M. Leung, *Astrophys. J.* **501**, 175 (1998).
13. H.-P. Gail and E. Sedlmayr, *Astron. Astrophys.* **132**, 163 (1984).
14. H.-P. Gail and E. Sedlmayr, *Astron. Astrophys.* **148**, 183 (1985).
15. J. H. Goebel and H. Moseley, *Astrophys. J. Lett.* **290**, L35 (1985).
16. J. M. Greenberg, *Interstellar Grains*, in *Stars and stellar systems*. Vol. VII, Ed. by B. M. Middlehurst and L. H. Aller (Univ. Chicago Press, p. 221, 1968; Mir, Moscow, 1970).
17. J. M. Greenberg, *Astron. Astrophys.* **12**, 240 (1971).
18. J. M. Greenberg and G. A. Shah, *Astron. Astrophys.* **12**, 250 (1971).
19. J. S. Hall, *Science* **109**, 166 (1949).
20. Th. Henning, V. B. Il'in, N. A. Krivova, B. Michel, N.V. Voshchinnikov, *Astron. Astrophys., Suppl. Ser.* **136**, 405 (1999).
21. R. H. Hildebrand, *Quart. J. R. A. S.* **24**, 267 (1983).
22. W. A. Hiltner, *Science* **109**, 165 (1949).
23. V. B. Il'in and N. V. Voshchinnikov, *Astron. Astrophys., Suppl. Ser.* **128**, 187 (1998).
24. C. Jäger, H. Mutshcke, B. Begemann, J. Dorschner, Th. Henning, *Astron. Astrophys.* **292**, 641 (1994).
25. C. Jäger, H. Mutschke, and Th. Henning, *Astron. Astrophys.* **332**, 291 (1998).
26. M. Jura, *Astrophys. J.* **434**, 713 (1994).
27. M. Jura, *Astrophys. J.* **472**, 806 (1996).

28. J.-P. J. Lafon and N. Berruyer, *Astron. Astrophys. Rev.* **2**, 249 (1991).
29. P. L. Lamy and J.-M. Perrin, *Astron. Astrophys.* **327**, 1147 (1997).
30. I. Little-Marenin, *Astrophys. J. Lett.* **307**, L15 (1986).
31. S. Lorenz-Martins and J. Lefèvre, *Astron. Astrophys.* **291**, 831 (1994).
32. J. S. Mathis, P. G. Mezger, and N. Panagia, *Astron. Astrophys.* **128**, 212 (1983).
33. T. Onaka, *Astrophys. J.* **533**, 298 (2000).
34. V. Ossenkopf and Th. Henning, *Astron. Astrophys.* **291**, 943 (1994).
35. V. Ossenkopf, Th. Henning, and J. S. Mathis, *Astron. Astrophys.* **261**, 567 (1992).
36. B. Pégourié, *Astrophys. Space Sci.* **136**, 133 (1987).
37. S. J. Shawl, *Astron. J.* **80**, 602 (1975).
38. R. Siebenmorgen, E. Krügel, and R. Chini, *Astron. Astrophys.* **351**, 495 (1999).
39. L. Spitzer, Jr., *Physical Processes in Interstellar Medium* (Wiley, New York, 1978; Mir, Moscow, 1981).
40. H. C. van de Hulst, *Rech. Astron. Obs. Utrecht* **11**, Part 2 (1949).
41. N. V. Voshchinnikov, *Itogi Nauki Tekh., Ser. Issled. Kosm. Prostranstva* **25**, 98 (1986).
42. N. V. Voshchinnikov and V. G. Farafonov, *Astrophys. Space Sci.* **204**, 19 (1993).
43. N. V. Voshchinnikov, D. A. Semenov, and Th. Henning, *Astron. Astrophys.* **349**, L25 (1999).
44. N. V. Voshchinnikov, V. B. Il'in, Th. Henning, B. Michel, V.G. Farafonov, *J. Quant. Spectrosc. Radiat. Transf.* **65**, 877 (2000).
45. L. B. F. M. Waters, F. J. Molster, and C. Waelkens, in *Solid Interstellar Matter: the ISO Revolution*, Ed. by L. d'Hendecourt *et al.* (Springer-Verlag, Berlin, 1999), p. 219.
46. D. C. B. Whittet, *Dust in the Galactic Environments* (Institute of Physics Publ., New York, 1992).
47. A. P. Whitworth, H. M. J. Boffin, and N. Francis, *Mon. Not. R. Astron. Soc.* **299**, 554 (1998).
48. P. Woitke, C. Dominik, and F. Sedlmayr, *Astron. Astrophys.* **274**, 451 (1993).

*Translated by V. Astakhov*